A CRLB for Passive Only TDOA Localization From a Three-Dimensional Hydrophone Array

Ryan Harvey† Krishna Pattipati† Peter Willett†

***Abstract*—This paper presents a mechanism for evaluating the Root Mean Square Error (RMSE) of a Minimum Variance Unbiased Estimator (MVUE) of a target state in 3D space using acoustic measurements. The target state is represented by (θ, ϕ, r) and it is estimated using Time Difference of Arrival measurements at the sensors and we assume that the sound-speed c is unknown. We then examine the interaction between azimuth angle θ on range RMSE, and the impacts of measurement noise variance on RMSE of (θ, ϕ, r, c) estimates. These results and analytical formulations can be used as a baseline to evaluate proper 3D array geometry design, as well as inform the potential RMSE improvements when using a biased minimum mean square error (MMSE) estimator over an unbiased (MVUE) one for the same set of measurements.**

***Index Terms*—target localization, target tracking, time difference of arrival, estimability, passive sensor localization, passive ranging, 3d array geometry, minimum variance unbiased estimator**

I. Introduction

Locating the source of an emitted signal is key in many areas of research, including wireless sensor networks [21], monitoring underwater infrastructure [23], tracking marine life [2], [27], and multi-object tracking with passive sensors [4]. Localization systems based on remote sensing can, in general, be divided into two categories: active sensing systems where the remote sensors transmit a known signal and localize the target based on the reflected energy, and passive sensing systems where the signal of interest is emitted solely by sources external to the sensor [4]. Active sensing systems typically result in a more straightforward localization process than passive systems; however, there are many domains where active sensing is either inappropriate or unavailable.

One of these domains where active sensing can be problematic is sonar. There is a significant evidence suggesting that the use of high powered active sonar systems can result in adverse effects on marine life [24], including posing a potentially serious risk to whale populations [20]. Beyond these ecological concerns, there are many domains like shallow water environments, where active sonar becomes problematic due to significant reverberation effects, thereby complicating the reflected signal [26]. Additionally, there are many use cases where active sonar strategies are inappropriate for use (e.g., covert submarine operation in the presence of anti-submarine warfare search strategies [12], [16]).

Work supported by the National Institute for Undersea Vehicle Technology under grant from the Office of Naval Research

† Dept. of Electrical and Computer Engineering, University of Connecticut, Storrs, CT 06029, USA.

⋆ Corresponding Author (email: ryan.harvey@uconn.edu)

In comparison, passive sensing can be applied in these areas but comes with challenging problems of its own. Many passive only sensing systems only provide reliable Direction of Arrival (DOA) measurements, resulting in the need for further Target Motion Analysis (TMA), to yield reliable range and position estimates of the object of interest [18]. In many cases, maintaining observability from bearings-only measurements requires complex maneuvers to be made by the sensing platform, and it is generally considered an intractable problem when the passive sensors are stationary [11].

Time-difference-of-arrival (TDOA) localization paradigms provide one of the key passive sonar measurement sources. A key question throughout the history of TDOA localization is concerned with full state observability/estimability from TDOA measurements and, in particular, the observability of target range from TDOA measurements. Examples of pioneering approaches to TDOA estimation with the goal of range observability include beam-forming based approaches [6], and hyperbolic location estimation [7]. Hyperbolic localization plays a major role in some recent TDOA acoustics works [10], [25], which leverage graph-based multi-target tracking and signal Doppler delay modeling, respectively, to produce reliable location estimates under their respective paradigms.

As an alternative to this hyperbolic approach, [19] presents a Nonlinear Programming (NLP) formulation for estimating the location, parameterized as (θ, ϕ, r), in the presence of uncertainty in the sound speed parameter c. This latter work expanded upon the work of [15], and sought to localize two surface vessels from real acoustic data gathered by a tetrahedral hydrophone array placed on the sea bed off the coast of Block Island. In particular, [19] presents a nonlinear least-squares (NLS) formulation for the simultaneous estimation of DOA (θ, ϕ), inverse range $\frac{1}{r}$, and sound speed c from a set of $N(N-1)/2$ TDOA measurements τ_{ij} which are assumed to be conditionally independent (following the convention of [8]). It was determined that 4 sensors are inadequate for accurate range estimation due to insufficient rank of the Hessian matrix; however, it is possible to estimate the inverse range with $N \geq 5$ sensors. Determining the optimal array design and performance evaluations of this NLP method for sensor arrays of $N \geq 5$ sensors is an open research problem.

This paper contributes the following, expanding upon [19]: Firstly, we formalize a joint likelihood function for the $N-1$ unique TDOA observations under the assumptions described in [19]. Secondly, we establish closed form expressions for the Fisher Information Matrix (FIM) elements, which can be used to determine the RMSE bounds for a Minimum Variance

Unbiased Estimator (MVUE) for the quantities $(\hat{\theta}, \hat{\phi}, \hat{r}, \hat{c})$ on a generic N sensor three-dimensional array. Thirdly, we examine the factors that impact this performance, including azimuth angle dependencies, true range dependencies, and the impact of RMSE in the time-of-arrival (TOA) measurements (i.e., noise variance) at each sensor. In a practical application of the estimator in [19], regularization strategies to address ill-conditioned Hessians and multiple initialization points will be needed due to multiple minima, making the unbiased MVUE bound not applicable due to the latter estimator being biased. However, the MVUE bound still provides a powerful baseline to evaluate whether biasing strategies like regularization are providing a benefit in terms of MSE over an ideal unbiased estimator of the same quantity. Additionally, this MVUE bound provides a useful evaluation of TDOA sensor array designs, giving a meaningful mechanism to analyze the performance both in an average case, and in the worst case target location geometry.

II. Problem Formulation

A. Probabilistic Model of Time of Arrival

Consider an array of N sensors at known positions given by $\{\underline{s}_i = \begin{bmatrix} x_i & y_i & z_i \end{bmatrix}^T : i = 1, 2, ..., N\}$ and define the center of the array location as $\overline{\underline{s}} = \begin{bmatrix} \overline{x} & \overline{y} & \overline{z} \end{bmatrix}^T$ such that

$$\overline{x} = \frac{1}{N}\sum_{i=1}^{N} x_i; \quad \overline{y} = \frac{1}{N}\sum_{i=1}^{N} y_i; \quad \overline{z} = \frac{1}{N}\sum_{i=1}^{N} z_i \tag{1}$$

Define the ensemble of vectors $\{\underline{\gamma}_i = \underline{s}_i - \overline{\underline{s}} : i = 1, 2, ..., N\}$ which give the relative displacement of sensor i with respect to the array center $\overline{\underline{s}}$. Assume that this sensor array is sitting on a solid surface (e.g., similar to [15]) such that no wave incidence occurs from below.

We let $\underline{x}_t = \begin{bmatrix} x & y & z \end{bmatrix}^T$ denote a target at a fixed but unknown position, and define the range from the target to the array center r to be the Euclidean distance $r = ||\underline{x}_t - \overline{\underline{s}}||$. Let $\underline{q}$ be the directional cosine vector $\underline{q}^T = \begin{bmatrix} u & v & w \end{bmatrix}$ where

$$u = \frac{x - \overline{x}}{r} = \cos(\theta)\sin(\phi) \tag{2}$$

$$v = \frac{y - \overline{y}}{r} = \sin(\theta)\sin(\phi) \tag{3}$$

$$w = \frac{z - \overline{z}}{r} = \cos(\phi) \tag{4}$$

where (θ, ϕ) are the respective azimuth and elevation angles of the target relative to the array center[1]. This is represented graphically in Fig. 1.

We assume a wave is emitted from the target $\underline{x}_t$ at an unknown time, propagating in a straight line at a constant speed c towards the sensor array, and is well approximated by a plane-wave at the Time of Arrival (TOA). Unlike in an active sensing regime where time-of-flight is observable, passive sensors can only detect the relative times of arrival [1].

[1]Note that in this formulation, we are assuming that the elevation angle ϕ is 0° when the target is directly above the array center and increases towards 90° as the target moves further away.

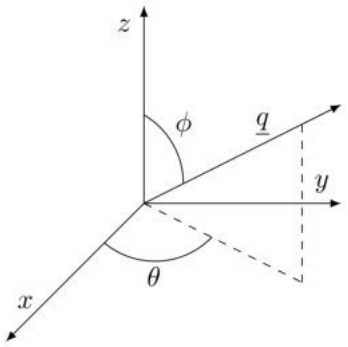

Fig. 1: Graphical depiction of the directional cosine vector $\underline{q}$

Given that we do not have time-of-flight information, we use a straight line approximation of direct path propagation between a point source and the known sensor array locations, which we always assume to be below the emission source, as it is on the sea floor. This approximation will likely not be an effective model in cases where highly complex wave propagation occurs, e.g., deep sound channel or bottom-bounce propagation [5], and other tools which deal with these scenario-specific complications will need to be utilized in these cases (e.g., matched-field processing (MFP) [28], time-reversal mirror (TRM) [13], or multi-path ranging [5]).

We denote the TOA of the plane-wave at sensor i to be t_i and it is given by:

$$t_i = \frac{||\underline{x}_t - \underline{s}_i||}{c} = \frac{||r\underline{q} - \underline{\gamma}_i||}{c} \tag{5}$$

This time of arrival will occur in the presence of measurement errors and will result in the (unobserved) random quantities

$$\tau_i = t_i + w_i \quad i = 1, 2, ..., N \tag{6}$$

where $w_i \sim \mathcal{N}(0, \sigma_i^2)$ is a zero-mean Gaussian random variable representing the errors made in the detection process. We model the $N \times 1$ random vector of TOA errors to be:

$$\underline{w} \sim \mathcal{N}(\underline{0}, \Sigma_w)$$

where Σ_w is an $N \times N$ covariance matrix. Then, we can model the observed $N - 1$ TDOA random variables via:

$$\begin{aligned} \tau_{12} &= \tau_2 - \tau_1 = (t_2 - t_1) + (w_2 - w_1) \\ \tau_{13} &= \tau_3 - \tau_1 = (t_3 - t_1) + (w_3 - w_1) \\ &\vdots \ \ \vdots \\ \tau_{1N} &= \tau_N - \tau_1 = (t_N - t_1) + (w_N - w_1) \end{aligned} \tag{7}$$

producing the joint likelihood function:

$$\Lambda(\underline{\tau}) = \mathcal{N}\left(\begin{bmatrix} z_{12} \\ \vdots \\ z_{1N} \end{bmatrix}; \begin{bmatrix} t_2 - t_1 \\ \vdots \\ t_N - t_1 \end{bmatrix}, D\Sigma_w D^T \right) \tag{8}$$

where

$$D = \begin{bmatrix} -\underline{1}_{N-1} & \underline{I}_{N-1\times N-1} \end{bmatrix} \tag{9}$$

and $\underline{1}_n$ represents the $n \times 1$ column vector with all entries being equal to 1, and $\underline{I}_{n\times n}$ is the $n \times n$ dimensional identity matrix.

The task then is specified as one of estimating the fixed but unknown parameters $(\hat{\theta}, \hat{\phi}, \hat{r}, \hat{c})$ from the joint distribution $p(\tau_{12}, ..., \tau_{1N})$, for which the NLS formulation given in [19] could be an example estimator.

Note that the TDOA process includes an implicit assumption that all of the arrival times are associated with the same plane wave incidence [1]. As a result, extension to cases where there is measurement origin uncertainty (MOU) in the (unobserved) TOA values is beyond the scope of this work.

B. Fisher Information Matrix

Using this representation of our noisy observations, the parametric likelihood function for a given TDOA observation set (denoted by $\underline{\tau}$) will be of the form given in (8).

The Cramér-Rao inequality [17] states that the covariance matrix of any unbiased estimator of the nonrandom (θ, ϕ, r, c) will be bounded below by the inverse of the Fisher Information Matrix (FIM) [3] given by

$$I = -\mathbb{E}\left[\nabla\nabla^T \ln(\Lambda(\underline{\tau}))\right]\Big|_{\underline{\tau}=\underline{\tau}_0} \tag{10}$$

where $\underline{\tau}_0$ corresponds to vector of "ground-truth" time differences and the gradient $\nabla \ln(\Lambda(\underline{\tau}))$ is taken with respect to the parameters (θ, ϕ, r, c). Given that the likelihood function for our observation $\underline{\tau}$ is a multivariate Gaussian, the FIM I will be given by [9]

$$I_{ij} = \frac{\partial \underline{\mu}^T}{\partial \lambda_i}\Sigma_\tau^{-1}\frac{\partial \underline{\mu}}{\lambda_j} + \frac{1}{2}\text{tr}\left[\Sigma_\tau^{-1}\frac{\partial \Sigma_\tau}{\partial \lambda_i}\Sigma_\tau^{-1}\frac{\partial \Sigma_\tau}{\partial \lambda_j}\right] \tag{11}$$

where $\underline{\lambda} = \begin{bmatrix}\theta, \phi, r, c\end{bmatrix}$ is the vector of parameters, and

$$\underline{\mu} = \mathbb{E}[\Lambda(\underline{\tau})], \quad \Sigma_\tau = D\Sigma_w D^T. \tag{12}$$

denote the mean and covariance matrix, respectively, of the observed TDOA joint likelihood function.

Note that in this case the covariance matrix Σ_τ does not have a dependence on the parameters we are seeking to estimate, so (11) simplifies to the quadratic product:

$$I_{ij} = \frac{\partial \underline{\mu}^T}{\partial \lambda_i}\Sigma_\tau^{-1}\frac{\partial \underline{\mu}}{\lambda_j} \tag{13}$$

The partial derivatives of t_i with respect to our parameters are given by

$$\frac{\partial t_i}{\partial \theta} = \frac{r}{c^2 t_i}\underline{q}^T(e_2 e_1^T - e_1 e_2^T)\underline{\gamma_i} \tag{14}$$

$$\frac{\partial t_i}{\partial \phi} = \frac{r}{c^2 t_i}\underline{q}^T \text{Diag}\left(\begin{bmatrix}-\cot(\phi)\\ -\cot(\phi)\\ \tan(\phi)\end{bmatrix}\right)\underline{\gamma}_i \tag{15}$$

$$\frac{\partial t_i}{\partial r} = \frac{\underline{q}^T(r\underline{q} - \underline{\gamma}_i)}{c^2 t_i} \tag{16}$$

$$\frac{\partial t_i}{\partial c} = \frac{-t_i}{c} \tag{17}$$

with proof of these partial derivatives given in Appendix A.

If the covariance matrix of the TOA errors, Σ_w, is non-diagonal, the inverse of the likelihood covariance matrix Σ_τ^{-1} has a complicated analytical form. In this case, one should use the Jacobian representation of the FIM I and evaluate it numerically:

$$I = \mathbf{J}^T(\underline{\mu})\Sigma_\tau^{-1}\mathbf{J}(\underline{\mu}) \tag{18}$$

where $\mathbf{J}(\underline{\mu})$ is the Jacobian matrix:

$$\mathbf{J}(\underline{\mu}) = \begin{bmatrix} \frac{\partial(t_2-t_1)}{\partial\theta} & \frac{\partial(t_2-t_1)}{\partial\phi} & \frac{\partial(t_2-t_1)}{\partial r} & \frac{\partial(t_2-t_1)}{\partial c} \\ \vdots & \vdots & \vdots & \vdots \\ \frac{\partial(t_N-t_1)}{\partial\theta} & \frac{\partial(t_N-t_1)}{\partial\phi} & \frac{\partial(t_N-t_1)}{\partial r} & \frac{\partial(t_N-t_1)}{\partial c} \end{bmatrix} \tag{19}$$

and $\Sigma_\tau^{-1} = (D\Sigma_w D^T)^{-1}$.

We will now present closed-form expressions for the FIM under two special cases (both of which assume that Σ_w is a diagonal matrix $\Sigma_w = \text{Diag}\left([\sigma_i^2]\right)$ for $i = 1, 2, ..., N$):

1) σ_i^2 is exactly known for all $i = 1, 2, ..., N$
2) $\sigma_i^2 \to \sigma^2$ for $i = 1, 2, ..., N$

where the second can be viewed as either an approximation of the first case, or a "worst-case" scenario with all of the TOA errors taking the value $\sigma^2 = \max_i\{\sigma_i^2\}$.

C. Special Case: σ_i^2 is exactly known

In the case that $\Sigma_w = \text{Diag}\left([\sigma_i^2]\right)$, $i = 1, 2, ..., N$, then we can decompose our covariance matrix Σ_τ into the following:

$$\Sigma_\tau = \text{Diag}\left(\begin{bmatrix}\sigma_2^2\\ \vdots \\ \sigma_N^2\end{bmatrix}\right) + \sigma_1^2\underline{1}_{N-1}\underline{1}_{N-1}^T \tag{20}$$

In this case, we can use the Sherman-Morrison-Woodbury Inverse identity [22] to produce

$$\Sigma_\tau^{-1} = \text{Diag}\left(\begin{bmatrix}\frac{1}{\sigma_2^2}\\ \vdots \\ \frac{1}{\sigma_N^2}\end{bmatrix}\right) - \frac{\sigma_1^2}{S}\begin{bmatrix}\frac{1}{\sigma_2^2}\\ \vdots \\ \frac{1}{\sigma_N^2}\end{bmatrix}\begin{bmatrix}\frac{1}{\sigma_2^2}\\ \vdots \\ \frac{1}{\sigma_N^2}\end{bmatrix}^T \tag{21}$$

where S is given by

$$S = \sum_{i=1}^{N}\frac{\sigma_1^2}{\sigma_i^2} \tag{22}$$

We can then use (21) along with (13) to produce a general form of the FIM I:

$$I = \mathbf{J}^T(\underline{\mu})\text{Diag}\left(\begin{bmatrix}\frac{1}{\sigma_2^2}\\ \vdots \\ \frac{1}{\sigma_N^2}\end{bmatrix}\right)\mathbf{J}(\underline{\mu}) - \frac{\sigma_1^2}{S}\mathbf{J}^T(\underline{\mu})\begin{bmatrix}\frac{1}{\sigma_2^2}\\ \vdots \\ \frac{1}{\sigma_N^2}\end{bmatrix}\begin{bmatrix}\frac{1}{\sigma_2^2}\\ \vdots \\ \frac{1}{\sigma_N^2}\end{bmatrix}^T\mathbf{J}(\underline{\mu}) \tag{23}$$

where $\mathbf{J}(\underline{\mu})$ is the Jacobian given in (19).

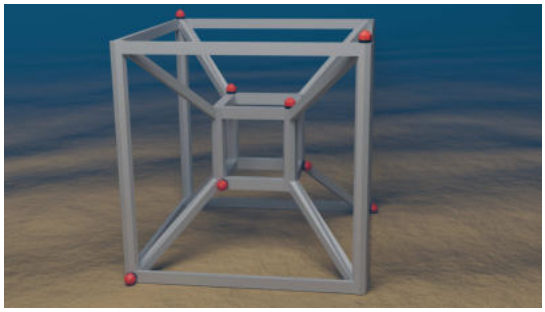

(a) Nested tetrehedral array design

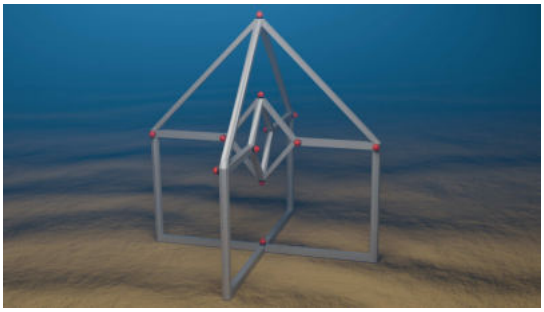

(b) Nested Octahedral Array Design

Fig. 2: Visualization of array designs 1 and 2 used in Sec. III. Outer sensor radius $0.75\sqrt{3}$m, inner sensor radius $0.25\sqrt{3}$m.

TABLE I: Hydrophone placement per sensor group for tetrahedral structure (top) and octahedral structure (bottom) parameterized on ρ. Each array has two groups, one outer group with ρ_1, and one inner group with ρ_2.

Coordinate/Sensor	1	2	3	4	5	6
x	ρ	$-\rho$	$-\rho$	ρ	-	-
y	ρ	$-\rho$	ρ	$-\rho$	-	-
z	ρ	ρ	$-\rho$	$-\rho$	-	-
x	$\rho\sqrt{3}$	$-\rho\sqrt{3}$	0	0	0	0
y	0	0	$\rho\sqrt{3}$	$-\rho\sqrt{3}$	0	0
z	0	0	0	0	$\rho\sqrt{3}$	$-\rho\sqrt{3}$

This form in terms of the Jacobian $\mathbf{J}(\underline{\mu})$ is already sufficient to implement numerically using (14)-(17); however, we will specify the explicit analytical sums in Appendix B. The FIM is guaranteed to be symmetric and positive semi-definite, and if we wish for all of the parameters to be observable, it must be positive definite [3].

In particular, we wish to examine the impact of our observation angles, range, and a measure of noise given a particular sensor array. This more general form allows for analysis in which each sensor has potentially varying quality (expressed via σ_i), lending itself to a variety of different problems including sensor selection when used on arrays with large N with variable per-sensor performance [14]. However, in many cases, the relationship between sensor quality and σ_i may be non-trivial or unobservable.

A common approximation for TDOA RMSE is given by:

$$\sigma_\tau \approx \frac{1}{2\pi \mathrm{BW}_{\mathrm{RMS}}\sqrt{\mathrm{SNR}}} \tag{24}$$

where $\mathrm{BW}_{\mathrm{RMS}}$ is the RMS bandwidth of the broadband signal prior to detection and SNR is the Signal-To-Noise ratio (signal variance vs. noise variance) at the time of detection [8].

Given that this SNR will depend on both the ambient environment and the quality/condition of the receivers, it may be necessary to approximate the TOA RMSE values by assuming a shared $\sigma = \frac{1}{2}\sigma_\tau$ based on the expected parameters for bandwidth and SNR.

D. Special Case: $\sigma_i^2 = \sigma^2\ \forall i \in \{1, 2, ..., N\}$

In the case of $\sigma_i^2 = \sigma^2$, $\forall i \in \{1, 2, ..., N\}$ we can simplify the expression (23) significantly.

This special case could represent a variety of approximations of the general case including:

$$\sigma^2 = \hat{\sigma}^2 = \frac{1}{N}\sum_{i=1}^{N}\sigma_i^2 \tag{25}$$

or

$$\sigma^2 = \max_{i\in\{1,2,...,N\}}(\sigma_i^2) \tag{26}$$

When all $\sigma_i^2 = \sigma^2$, we have that:

$$\Sigma^{-1} = \frac{1}{\sigma^2}\underline{I}_{N-1\times N-1} - \frac{1}{N\sigma^2}\underline{1}_{N-1\times N-1}. \tag{27}$$

As a result, the expressions (35)-(44) become greatly simplified, as we can factor $\frac{1}{\sigma^2}$ out of all terms. Doing so yields the interpretation that our Fisher Information for each term is inversely proportional to the shared TOA MSE σ^2, and that the cross terms in their respective expressions will diminish in contribution as the number of sensors, N, grows.

III. Results

There are a number of potential factors that will impact the performance of an MVUE in this scenario on the four parameters that one would wish to estimate. For brevity, we will primarily focus on the MVUE RMSE for range, as it is the primary quantity in the parameter set (θ, ϕ, r, c) for which existing passive TDOA estimation schemes struggle. When applicable, we will compare the MVUE RMSE quantities to Monte Carlo (MC) trials using the NLS estimator given in [19]. However, the estimator functions best when using regularization strategies, which minimize the mean square error (MSE) by introducing a bias in the estimate at a substantial reduction in variance and make the MVUE-based CRLB an inappropriate lower bound for comparison.

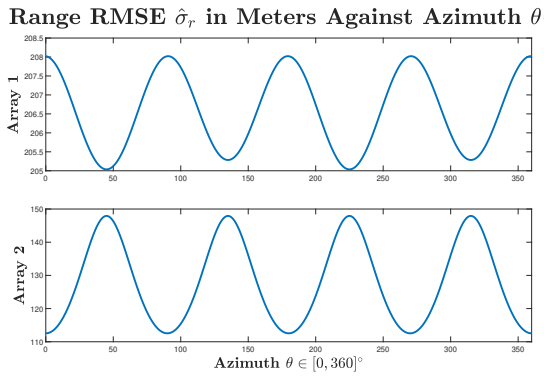

(a) MVUE range RMSE against azimuth θ

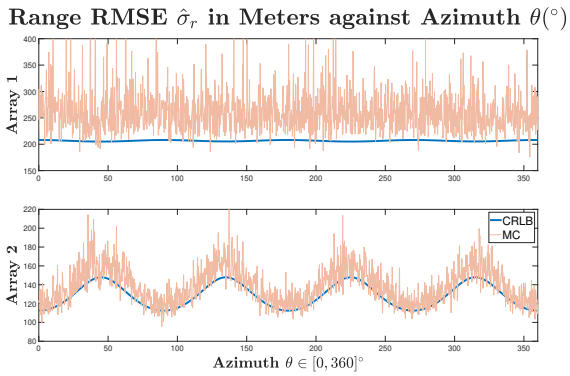

(b) Realized MC trials using NLS estimator [19] for Scenario 1

Fig. 3: Azimuth dependence of MVUE range RMSE $\hat{\sigma}_r$, Array 1 (top), Array 2 (bottom) for Scenario 1

TABLE II: Maximum and minimum MVUE RMSE over the angular sweep $\phi \in [86.5, 89.5]^\circ$, $\theta \in [0, 360]^\circ$

	$\max \hat{\sigma}_\theta(^\circ)$	$\min \hat{\sigma}_\theta(^\circ)$	$\max \hat{\sigma}_\phi(^\circ)$	$\min \hat{\sigma}_\phi(^\circ)$	$\max \hat{\sigma}_c$ (m/s)	$\min \hat{\sigma}_c$ (m/s)
Array 1:	$9.36 \cdot 10^{-5}$	$9.30 \cdot 10^{-5}$	$1.33 \cdot 10^{-2}$	$1.60 \cdot 10^{-3}$	$2.29 \cdot 10^{-1}$	$1.95 \cdot 10^{-1}$
Array 2:	$7.61 \cdot 10^{-5}$	$7.60 \cdot 10^{-5}$	$8.60 \cdot 10^{-3}$	$1.30 \cdot 10^{-3}$	$1.69 \cdot 10^{-1}$	$1.60 \cdot 10^{-1}$

TABLE III: Scenario 1 parameters

r (m)	c (m/s)	$\phi(^\circ)$	ρ_1 (m)	ρ_2 (m)	σ_τ (s)
1000	1471	88.25	0.75	0.25	10^{-7}

While in principle there are a large number of factors that could be explored in the design of the array, we will be generating results on the following array structures:

- Array 1: 8 sensor nested tetrahedral array
- Array 2: 12 sensor nested octahedral array

where both arrays are designed such that their sensors are on the same concentric spheres of radii $\sqrt{3}\rho_1$, $\sqrt{3}\rho_2$ respectively. Visualizations of these arrays are given in Figs. 2a-2b, and the placement of the groups of sensors parameterized on ρ is given in Table I.

A. Observation Angle Dependencies

Here we will focus on ground truth geometries that are similar to the scenario in [19], where the sensor array is placed at a depth that is similar to a shallow sea-bed (approximately 30 meters) and focusing on simulated targets that are within 3km of the array. In this scenario, the elevation angle will be constrained to the interval $\phi \in [86.5, 89.5]^\circ$, and the two sensor geometries have very little variation in range RMSE with respect to elevation angle. For any particular θ, the performance difference $|\max_\phi \hat{\sigma}_r(\phi, \theta) - \min_\phi \hat{\sigma}_r(\phi, \theta)| \approx 0.5$m in the cases we examined, whereas the variation in $\hat{\sigma}_r$ against θ is typically much larger.

This variation in $\hat{\sigma}_r$ against θ (for the scenario given in Table III) is illustrated in Fig. 3a. In this scenario the nested octahedral array outperforms the nested tetrahedral array in terms of range RMSE at all azimuth angles (despite being constrained to the same spherical volume). However, the nested tetrahedral array, despite performing worse in both the best observation angles and worst observation angles, has significantly less variability in performance than the nested octahedral array. Thus one should expect that while the octahedral array of the same volume will deliver lower range RMSE, it will have far more variability in performance at different observation angles.

For numerical validation, MC trials were conducted for Scenario 1 (given in Table III) with the variable $\theta \in [0, 360]$ varying with $\Delta\theta = 0.25^\circ$ increments. 150 trials were conducted per $\Delta\theta$, with randomness occuring in two sources, the TOA errors and the initialization point for the NLS estimator. MATLAB's optimization toolkit was used for solution of these NLS estimates using the sequential quadratic programming (SQP) routine with constraints as described in [19].

Examining the realized Monte Carlo trials shown in 3b, Array 2 generally outperforms Array 1 both in numerical values and estimator stability despite having the same minimum and maximum array radii. Given (27) shows an increase in precision as the number of sensors N grows, this is likely due to the additional 4 sensors in Array 2 relative to Array 1.

These trials show that in some circumstances, the estimator proposed in [19] can achieve near optimal sample RMSE; however, the estimator proposed in [19] requires additional constraints which may introduce bias in cases where the problem is ill-conditioned (as is the case when r or σ_τ grow large).

As shown in Fig. 4a this variability produces significant differences in $\hat{\sigma}_r$ as the true range increases. In particular, for the nested octahedral array, $\frac{\max_\theta \hat{\sigma}_r}{\min_\theta \hat{\sigma}_r} \approx 1.315$, so one would expect that as r increases, the impact of observation angle will become relevant to the viability in a single unbiased estimate (θ, ϕ, r) being used as input to a tracking system.

The impacts of observation angle on $\hat{\sigma}_\theta$, $\hat{\sigma}_\phi$, and $\hat{\sigma}_c$ are substantially smaller than for the range, and are presented for

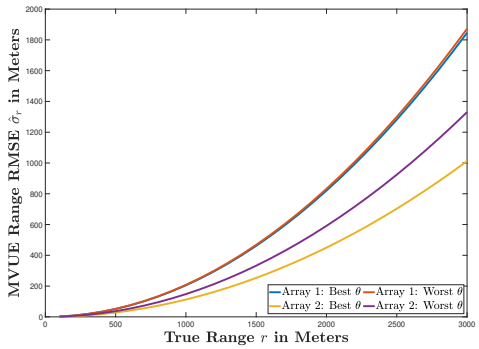

(a) MVUE range RMSE $\hat{\sigma}_r$ against true range

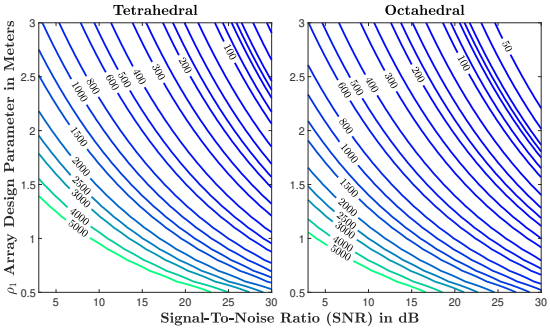

(b) MVUE $\hat{\sigma}_r$ (m) against ρ_1 (m) and Signal-to-Noise Ratio (dB) for a target at 3000m range with 40kHz RMS Bandwidth, $\rho_2 = 0.25$m, $c = 1471$m/s, Array 1 (left), Array 2 (right)

Fig. 4: Impacts of true range, array size ρ_1, and SNR on MVUE range RMSE $\hat{\sigma}_r$.

the same array as used in Fig. 3a over the angular sweep $\phi \in [86.5, 89.5]$, $\theta \in [0, 360]$ in Table II.

B. Scaling Against Range and σ_τ

As range increases, with a fixed size array and fixed TDOA noise variance σ, the quantity $\hat{\sigma}_r$ will increase significantly. This is a function primarily of the geometry of the problem, and in many ways is not rectifiable without achieving a better σ value, increasing the size of the array, or regularization and multi-start optimization.

The estimation strategy given in [19] becomes significantly ill conditioned as r grows larger, which may be mediated by regularization strategies or median filtering of consecutive estimates (at the cost of introducing a bias into the estimate). The quantities $\hat{\sigma}_\theta$, $\hat{\sigma}_\phi$, and $\hat{\sigma}_c$ are all improved by increased range, and are reliably estimable in the short ranges where $\hat{\sigma}_r$ is reasonable (as shown in Table II).

Similarly, with a fixed range r, an increased σ will significantly increase the MVUE $\hat{\sigma}_r$. Given that it is not usually known exactly what σ will be for any particular sensor, we will instead use (24) specify the performance against σ in terms of SNR. Fig. 4b presents the case where $\text{BW}_{\text{RMS}} = 40$ kHz, the target is at 3000m range and examines the impact of increasing the array size via ρ_1 at various levels of SNR. It is clear that unless the array is allowed to grow to significant sizes, either a very high bandwidth or very high SNR are needed for a reasonable $\hat{\sigma}_r$ under these conditions. However, if the application allows for arrays larger than 1m, moderate increases in size can yield significant improvement in MVUE range RMSE.

IV. Conclusions and Future Work

This work developed and examined MVUE bounds for estimation of the target and environment parameters $(\hat{\theta}, \hat{\phi}, \hat{r}, \hat{c})$ based on TDOA observations from an array with arbitrary 3d sensor geometry. These bounds can be used both as a baseline for the evaluation of TDOA estimators of these quantities, as well as for evaluation of sensor geometry performance under a variety of observation conditions. For the particular use case we examined, azimuth angle plays a large role in the estimation of $\hat{r}$, and this bound can inform the design of TDOA arrays in terms of both average performance, and robustness to unfortunate true target locations.

In addition, these MVUE bounds can inform array design when particular SNR and true range pairs are specified, allowing for a meaningful metric on passive TDOA ranging performance for a particular array size. This metric can be used to make informed decisions on the smallest possible array of a particular configuration when $\hat{\sigma}_r$, r, and SNR are specified. This is array design benefit is extended further if a particular set of per-sensor σ_i values are specified, corresponding to the design of arrays with potentially varying sensor quality.

Examination of the MVUE bounds for an estimator of the parameters $(\hat{\theta}, \hat{\phi}, \hat{r}, \hat{c})$ indicates that an unbiased estimator may not be appropriate for passive ranging in many circumstances where this could be applied. In particular, if either the range is too large or the SNR is too small, the array dimensions need to grow considerably for range estimates to have an RMSE that could be reasonably used as input to a tracking system.

One particular method of addressing this problem is to introduce regularization (or shrinkage) into the cost function of the estimator given in [19]. This approach will introduce a bias, as it implies a prior on the parameter r; however it should allow for a lower MSE estimate of $\hat{r}$ under a wider range of true state conditions.

Additionally, given the transformation from t_i to (θ, ϕ, r_i, c) is highly nonlinear, any practical estimator of $(\hat{\theta}, \hat{\phi}, \hat{r}, \hat{c})$ will require either some prior knowledge of an appropriate initialization point (e.g., from the previous state estimate if used in conjunction with a tracker), or multiple starting points and selecting the best estimate based on the objective function.

Future efforts will focus on determining the most appropriate regularization strategies for an estimator of the target state, as well as incorporation of multiple measurement sources of this type into a tracking system. The impact of the estimation bias introduced by this regularization will be examined, as well as the tracking performance in a fusion system with multiple measurement sources of this type.

APPENDIX A
PARTIAL DERIVATIVES OF t_i

Let t_i be defined via:

$$t_i = \frac{||r\underline{q} - \underline{\gamma}_i||_2}{c}$$

where

$$\underline{q} = \begin{bmatrix}\cos(\theta)\sin(\phi) & \sin(\theta)\sin(\phi) & \cos(\phi)\end{bmatrix}^T$$

and $\underline{\gamma}_i$ and r are as described in II-A.

The partial derivatives $\frac{\partial t_i}{\partial \theta}$, $\frac{\partial t_i}{\partial \phi}$, and $\frac{\partial t_i}{\partial r}$ all have components inside of the Euclidean norm, and as a result will take the forms:

$$\frac{\partial t_i}{\partial \theta} = \frac{1}{2c||r\underline{q} - \underline{\gamma}_i||_2}\frac{\partial}{\partial \theta}\left\{r\underline{q} - \underline{\gamma}_i\right\} \tag{28}$$

$$\frac{\partial t_i}{\partial \phi} = \frac{1}{2c||r\underline{q} - \underline{\gamma}_i||_2}\frac{\partial}{\partial \phi}\left\{r\underline{q} - \underline{\gamma}_i\right\} \tag{29}$$

$$\frac{\partial t_i}{\partial r} = \frac{1}{2c||r\underline{q} - \underline{\gamma}_i||_2}\frac{\partial}{\partial r}\left\{r\underline{q} - \underline{\gamma}_i\right\} \tag{30}$$

Given that $t_i = ||r\underline{q} - \underline{\gamma}_i||_2/c$, we have

$$||r\underline{q} - \underline{\gamma}_i||_2 = ct_i$$

meaning (28)-(30) have denominator $2c^2t_i$.

Some standard calculus will yield:

$$\begin{aligned}\frac{\partial}{\partial \theta}\left\{r\underline{q} - \underline{\gamma}_i\right\} &= 2r\sin(\theta)\sin(\phi)(x_i - \overline{x}) \\ &\quad - 2r\cos(\theta)\sin(\phi)(y_i - \overline{y}) \\ &= 2r\underline{q}^T(e_2e_1^T - e_1e_2^T)\underline{\gamma}_i\end{aligned} \tag{31}$$

Similarly for ϕ:

$$\begin{aligned}\frac{\partial}{\partial \phi}\left\{r\underline{q} - \underline{\gamma}_i\right\} &= -2r\cos(\theta)\cos(\phi)(x_i - \overline{x}) \\ &\quad - 2r\sin(\theta)\cos(\phi)(y_i - \overline{y}) \\ &\quad + 2r\sin(\phi)(z_i - \overline{z}) \\ &= 2r\underline{q}^T\text{Diag}\left(\begin{bmatrix}-\cot(\phi) \\ -\cot(\phi) \\ \tan(\phi)\end{bmatrix}\right)\underline{\gamma}_i\end{aligned} \tag{32}$$

and for r:

$$\begin{aligned}\frac{\partial}{\partial r}\left\{r\underline{q} - \underline{\gamma}_i\right\} &= 2r - 2\underline{q}^T\underline{\gamma}_i \\ &= 2(r - \underline{q}^T\underline{\gamma}_i) \\ &= 2\underline{q}^T(r\underline{q} - \underline{\gamma}_i)\end{aligned} \tag{33}$$

via $\underline{q}^T\underline{q} = 1$.

Substitution of (31)-(33) into their respective equations in (28)-(30) yields the final expressions given in (14)-(16).

For $\frac{\partial t_i}{\partial c}$, we have:

$$\frac{\partial t_i}{\partial c} = -\frac{||r\underline{q} - \underline{\gamma}_i||_2}{c^2} = -\frac{t_i}{c} \tag{34}$$

This completes the proof of the partial derivative expressions (14)-(17).

APPENDIX B
EXPLICIT FIM ANALYTICAL EXPRESSIONS

There will be 10 unique entries in the FIM, whose analytical form for the special case of Sec. II-A is given below:

$$\begin{aligned}I_{11} &= -\mathbb{E}\left[\frac{\partial^2 \ln(\Lambda(\underline{\tau}))}{\partial \theta^2}\right] \\ &= \sum_{j=2}^{N}\frac{r^2}{c^4\sigma_j^2}\underline{\delta}_{1j}^T\mathbf{M}(\theta,\phi)\underline{\delta}_{1j} - \frac{\sigma_1^2}{S}\left(\sum_{k=2}^{N}\frac{r\underline{q}^T\mathbf{P}\underline{\delta}_{1k}}{c^2\sigma_k^2}\right)^2\end{aligned} \tag{35}$$

$$\begin{aligned}I_{12} &= -\mathbb{E}\left[\frac{\partial^2 \ln(\Lambda(\underline{\tau}))}{\partial \theta \partial \phi}\right] \\ &= \sum_{j=2}^{N}\frac{r^2}{c^4\sigma_j^2}\underline{\delta}_{1j}^T\mathbf{R}(\theta,\phi)\underline{\delta}_{1j} \\ &\quad - \frac{\sigma_1^2}{S}\left(\sum_{k=2}^{N}\frac{r\underline{q}^T\mathbf{P}\underline{\delta}_{1k}}{c^2\sigma_k^2}\right)\left(\sum_{k=2}^{N}\frac{r\underline{q}^T\mathbf{T}(\phi)\underline{\delta}_{1k}}{c^2\sigma_k^2}\right)\end{aligned} \tag{36}$$

$$\begin{aligned}I_{13} &= -\mathbb{E}\left[\frac{\partial^2 \ln(\Lambda(\underline{\tau})))}{\partial \theta \partial r}\right] \\ &= \sum_{j=2}^{N}\frac{r}{c^4\sigma_j^2}\underline{\delta}_{1j}^T\mathbf{G}(\theta,\phi)\underline{\xi}_{1j} \\ &\quad - \frac{\sigma_1^2}{S}\left(\sum_{k=2}^{N}\frac{r\underline{q}^T\mathbf{P}\underline{\delta}_{1k}}{c^2\sigma_k^2}\right)\left(\sum_{k=2}^{N}\frac{\underline{q}^T\underline{\xi}_{1k}}{c^2\sigma_k^2}\right)\end{aligned} \tag{37}$$

$$\begin{aligned}I_{14} &= -\mathbb{E}\left[\frac{\partial^2 \ln(\Lambda(\underline{\tau}))}{\partial \theta \partial c}\right] \\ &= -\sum_{j=2}^{N}\frac{r(t_j - t_1)}{c^3\sigma_j^2}\underline{q}^T\mathbf{P}\underline{\delta}_{1j} \\ &\quad + \frac{\sigma_1^2}{S}\left(\sum_{k=2}^{N}\frac{r\underline{q}^T\mathbf{P}\underline{\delta}_{1k}}{c^2\sigma_k^2}\right)\left(\sum_{k=2}^{N}\frac{t_k - t_1}{c\sigma_k^2}\right)\end{aligned} \tag{38}$$

$$\begin{aligned}I_{22} &= -\mathbb{E}\left[\frac{\partial^2 \ln(\Lambda(\underline{\tau}))}{\partial \phi^2}\right] \\ &= \sum_{j=2}^{N}\frac{r^2}{c^4\sigma_j^2}\underline{\delta}_{1j}^T\mathbf{\Phi}(\theta,\phi)\underline{\delta}_{1j} - \frac{\sigma_1^2}{S}\left(\sum_{k=2}^{N}\frac{r\underline{q}^T\mathbf{T}(\phi)\underline{\delta}_{1k}}{c^2\sigma_k^2}\right)^2\end{aligned} \tag{39}$$

$$\begin{aligned}I_{23} &= -\mathbb{E}\left[\frac{\partial^2 \ln(\Lambda(\underline{\tau}))}{\partial \phi \partial r}\right] \\ &= \sum_{j=2}^{N}\frac{r}{c^2\sigma_j^2}\underline{\delta}_{1j}^T\mathbf{L}(\theta,\phi)\underline{\xi}_{1j} \\ &\quad - \frac{\sigma_1^2}{S}\left(\sum_{k=2}^{N}\frac{r\underline{q}^T\mathbf{T}(\phi)\underline{\delta}_{1j}}{c^2\sigma_k^2}\right)\left(\sum_{k=2}^{N}\frac{\underline{q}^T\underline{\xi}_{1j}}{c^2\sigma_k^2}\right)\end{aligned} \tag{40}$$

$$\begin{aligned}I_{24} &= -\mathbb{E}\left[\frac{\partial^2 \ln(\Lambda(\underline{\tau}))}{\partial \phi \partial c}\right] \\ &= -\sum_{j=2}^{N}\frac{r(t_j - t_1)\underline{q}^T\mathbf{T}(\phi)\underline{\delta}_{1j}}{c^3\sigma_j^2} \\ &\quad + \frac{\sigma_1^2}{S}\left(\sum_{k=2}^{N}\frac{r\underline{q}^T\mathbf{T}(\phi)\underline{\delta}_{1k}}{c^2\sigma_k^2}\right)\left(\sum_{k=2}^{N}\frac{t_k - t_1}{c\sigma_k^2}\right)\end{aligned} \tag{41}$$

$$I_{33} = -\mathbb{E}\left[\frac{\partial^2 \ln(\Lambda(\underline{\tau}))}{\partial r^2}\right] = \sum_{j=2}^{N} \frac{\underline{\xi}_{1j}^T \underline{q}\underline{q}^T \underline{\xi}_{1j}}{c^4\sigma_j^2} - \frac{\sigma_1^2}{S}\left(\sum_{k=2}^{N} \frac{\underline{q}^T \underline{\xi}_{1k}}{c^2\sigma_k^2}\right)^2 \quad (42)$$

$$I_{34} = -\mathbb{E}\left[\frac{\partial^2 \ln(\Lambda(\underline{\tau}))}{\partial r \partial c}\right] = -\sum_{j=2}^{N} \frac{(t_j - t_1)\underline{q}^T \underline{\xi}_{1j}}{c^3\sigma_j^2} + \frac{\sigma_1^2}{S}\left(\sum_{k=2}^{N} \frac{\underline{q}^T \underline{\xi}_{1k}}{c^2\sigma_k^2}\right)\left(\sum_{k=2}^{N} \frac{t_k - t_1}{c\sigma_k^2}\right) \quad (43)$$

$$I_{44} = -\mathbb{E}\left[\frac{\partial^2 \ln(\Lambda(\underline{\tau}))}{\partial c^2}\right] = \sum_{j=2}^{N} \frac{(t_j - t_1)^2}{c^2\sigma_j^2} - \frac{\sigma_1^2}{S}\left(\sum_{k=2}^{N} \frac{t_k - t_1}{c\sigma_k^2}\right)^2 \quad (44)$$

where

$$\mathbf{T}(\phi) = \text{Diag}\left(\begin{bmatrix} -\cot(\phi) & -\cot(\phi) & \tan(\phi) \end{bmatrix}\right)$$

$$\underline{\delta}_{ij} = \frac{t_i\underline{\gamma}_j - t_j\underline{\gamma}_i}{t_i t_j}, \quad \underline{\xi}_{ij} = \frac{t_i(r\underline{q} - \underline{\gamma}_j) - t_j(r\underline{q} - \underline{\gamma}_i)}{t_i t_j}$$

$$\begin{aligned} \mathbf{P} &= e_2 e_1^T - e_1 e_2^T, & \mathbf{M}(\theta,\phi) &= \mathbf{P}^T \underline{q}\underline{q}^T \mathbf{P} \\ \mathbf{R}(\theta,\phi) &= \mathbf{P}^T \underline{q}\underline{q}^T \mathbf{T}(\phi), & \mathbf{G}(\theta,\phi) &= \mathbf{P}^T \underline{q}\underline{q}^T \\ \mathbf{\Phi}(\theta,\phi) &= \mathbf{T}(\phi)\underline{q}\underline{q}^T \mathbf{T}(\phi), & \mathbf{L}(\theta,\phi) &= \mathbf{T}(\phi)\underline{q}\underline{q}^T \end{aligned} \quad (45)$$

The exact values of this FIM will be contingent on the particular ground-truth (θ, ϕ, r, c), the geometry of the sensor arrays, and the TOA RMSE associated with each sensor.

REFERENCES

[1] D. A. Abraham, *Underwater Acoustic Signal Processing*, 1st ed. Springer CHAM, 2019.

[2] J. L. Amaral, J. H. Miller, G. R. Potty, Y.-T. Lin, and K. J. Vigness-Raposa, "Fin whale localization and environmental inversion using modal arrivals of the 20-hz pulse," *The Journal of the Acoustical Society of America*, vol. 150, no. 4-S, pp. A201–A201, 10 2021.

[3] Y. Bar-Shalom, X. R. Li, and T. Kirubarajan, *Estimation with Applications to Tracking and Navigation*. Wiley Interscience, 2001.

[4] Y. Bar-Shalom, P. K. Willett, and X. Tian, *Tracking and Data Fusion*. YBS Publishing, 2011.

[5] W. S. Burdic, *Underwater Acoustic System Analysis*, 2nd ed. Prentice Hall, 1991.

[6] C. G. Carter, "Time delay estimation for passive sonar signal processing," *IEEE Transactions on Acoustics, Speech, and Signal Processing*, vol. 29, no. 3, 06 1981.

[7] Y. T. Chan and K. C. Ho, "A simple and efficient estimator for hyperbolic location," *IEEE Transactions On Signal Processing*, vol. 42, no. 8, pp. 1905–1911, 08 1994.

[8] R. B. Gampert, "Development of an acoustic tracking system for harbor porpoises in the vicinity of gill nets," Master's thesis, University of Rhode Island, Department of Ocean Engineering, 1998.

[9] S. M. Kay, *Fundamentals of Statistical Signal Processing: Estimation Theory*. Prentice Hall, 1993.

[10] B. Kouzoundjian, F. Beaubois, S. Reboul, J. Bernard Choquel, and J.-C. Noyer, "A tdoa underwater localization approach for shallow water environment," in *OCEANS 2017 - Aberdeen*, 2017, pp. 1–4.

[11] J. E. Le Cadre and C. Jauffret, "Discrete-time observability and estimability analysis for bearings-only target motion analysis," *IEEE Transactions on Aerospace and Electronic Systems*, vol. 33, no. 1, pp. 178–201, 1997.

[12] K. D. LePage, M. Oddone, M. Micheli, T. Fabbri, and G. Ferri, "Environmental services embedded on maritime unmanned systems for asw decision support," in *OCEANS 2021: San Diego – Porto*, 2021, pp. 1–7.

[13] K.-W. Liu, C.-J. Huang, G.-P. Too, Z.-Y. Shen, and Y.-D. Sun, "Underwater sound source localization based on passive time-reversal mirror and ray theory," *sensors*, vol. 22, no. 6, 2022. [Online]. Available: https://www.mdpi.com/1424-8220/22/6/2420

[14] S. Liu, S. P. Chepuri, M. Fardad, E. Maşazade, G. Leus, and P. K. Varshney, "Sensor selection for estimation with correlated measurement noise," *IEEE Transactions on Signal Processing*, vol. 64, no. 13, pp. 3509–3522, 2016.

[15] J. H. Miller, G. R. Potty, A. Tripathy, M. Tazawa, J. Amaral, K. J. Vigness-Raposa, Y.-T. Lin, and A. Newhall, "Source localization using a compact tetrahedral array," *The Journal of the Acoustical Society of America*, vol. 144, no. 3, pp. 1745–1745, 2018. [Online]. Available: https://doi.org/10.1121/1.5067739

[16] M. Mishra, W. An, D. Sidoti, X. Han, D. F. M. Ayala, J. A. Hansen, K. R. Pattipati, and D. L. Kleinman, "Context-aware decision support for anti-submarine warfare mission planning within a dynamic environment," *IEEE Transactions on Systems, Man, and Cybernetics: Systems*, vol. 50, no. 1, pp. 318–335, 2020.

[17] N. Mukhopadhyay, *Probability and Statistical Inference*. Marcel Dekker, 2000.

[18] S. C. Nardone, A. G. Lindgren, and K. F. Gong, "Fundamental properties and performance of conventional bearings-only target motion analysis," *IEEE Transactions on Automatic Control*, vol. 29, no. 9, pp. 775–787, sep 1948.

[19] C. Norton, R. Harvey, J. MIller, P. Willett, L. Zhang, and K. Pattipati, "Computational algorithms for acoustic signals direction of arrival and sound speed estimation," in *2023 26th International Conference on Information Fusion (FUSION)*, 2023, pp. 1–7.

[20] E. C. M. Parsons, "Impacts of navy sonar on whales and dolphins: Now beyond a smoking gun?" *Frontiers in Marine Science*, vol. 4, 2017.

[21] A. K. Paul and T. Sato, "Localization in wireless sensor networks: A survey on algorithms, measurement techniques, applications and challenges," *Journal of Sensor and Actuator Networks*, vol. 6, no. 4, sep 2017.

[22] K. B. Petersen and M. S. Pedersen, "The matrix cookbook," p. 18, nov 2012. [Online]. Available: http://www2.compute.dtu.dk/pubdb/pubs/3274-full.html

[23] G. Soldi, D. Gaglione, S. Raponi, N. Forti, E. d'Afflisio, P. Kowalski, L. M. Millefiori, D. Zissis, P. Braca, P. Willett, A. Maguer, S. Carniel, G. Sembenini, and C. Warner, "Monitoring of critical undersea infrastructures: The nord stream and other recent case studies," *IEEE Aerospace and Electronic Systems Magazine*, vol. 38, no. 10, pp. 4–24, 2023.

[24] B. L. Southall, A. E. Bowles, W. T. Ellison, J. J. Finneran, R. L. Gentry, C. R. Greene Jr., D. Kastak, D. R. Ketten, J. H. Miller, P. E. Nachtigall, W. J. Richardson, J. A. Thomas, and P. L. Tyack, "Marine mammal noise exposure criteria: initial scientific recommendations (2007)," *Aquatic Mammals*, vol. 33, pp. 1–121, 2007.

[25] A. Tesei, F. Meyer, and R. Been, "Tracking of multiple surface vessels based on passive acoustic underwater arrays," *The Journal of the Acoustical Society of America*, vol. 147, no. 2, pp. 87–92, 02 2020.

[26] R. J. Urick, *Principles of Underwater Sound*, 2nd ed. McGraw-Hill, 1975.

[27] G. A. Warner, S. E. Dosso, and D. E. Hannay, "Bowhead whale localization using time-difference-of-arrival data from asynchronous recorders," *The Journal of the Acoustical Society of America*, vol. 141, no. 3, pp. 1921–1935, 03 2017.

[28] D. Zhao, W. Seong, K. Lee, and Z. Huang, "Shallow water source localization using a mobile short horizontal array," *Journal of Systems Engineering and Electronics*, vol. 24, no. 5, pp. 749–760, 2013.